BER the international journal of bridge engineering management and research

Experimental Investigation of the Grouted Shear Stud Connection and a Mechanics-Based Model for Minimum Connection Capacity

Arjun Jayaprakash*; James M. Nau; Mervyn J. Kowalsky; and Mohammad Pour-Ghaz

Submitted: 17 February 2025 **Accepted:** 26 March 2025 **Publication date:** 10 April 2025

DOI: 10.70465/ber.v2i2.25

Abstract: The grouted shear stud (GSS) connection is a ductile detail suitable for the seismic design of pile-to-cap-beam connections in bridges, piers, and marginal wharves. It is constructed by inserting the pile into an external socket attached to the cap beam and subsequently grouting the annular void thus formed. Previous research has shown that the GSS connection can successfully relocate damage to the columns in the form of plastic hinge formation, thereby mobilizing the full strength and ductility capacity of the system. However, no prior studies have investigated the force-transfer mechanism inside the connection. As a result, a standard approach for designing an optimal connection does not exist. To better understand the force-transfer mechanism, an experimental study was undertaken. Four large-scale two-column steel bridge bent specimens were structurally tested under cyclic lateral loading. It was found that the embedment length of the column inside the connection is the most critical parameter for a successful design. An a priori model based on a truss mechanism was developed to calculate the lower bound capacity of the GSS connection. A comparison with experimental results shows that the model can be used to ensure that the GSS connection remains capacity protected under seismic loading.

Author keywords: Grouted Shear Stud Connection; Large-scale Experiments; Ductile Bridge Substructure; Connection Design

Introduction

The use of structural systems consisting of circular steel piles doubling as columns above ground has been widespread in bridges, piers, and marginal wharves.[1–6] In bridges, these pile columns are used as part of bridge bents, which are located at intermittent points along the length of the bridge, often marking the endpoints of bridge girders. In these structures, the piles are often made of hollow or concrete-filled steel tubes. Drilled or driven piles are erected and cut at the same elevation before connecting to the cap beam. The cap beam is either made of structural steel[5] or reinforced concrete (RC).[4]

In the case of a steel pile-to-steel cap-beam connection, the traditional construction approach has been to directly weld the two members together.[1,5,7] Directly welded connections have been shown to undergo brittle failure modes, such as weld fracture, even at low levels of inelastic action.[1,7]

External socket connections have emerged as improved alternatives for fabricating the connection between piles and cap elements.[8,9] Typically, these involve a structural socket attached to the exterior of the adjoining member into which the piles can be inserted. The annular void thus generated can then be filled with a high-strength grout material.

One example of an external socket connection is the grouted shear stud (GSS) connection, developed at North Carolina State University.[9] While originally developed for use in steel bridges in Alaska, the GSS connection can also be extended for use in other structures such as RC columns or concrete-filled steel tubes.[10] Because the GSS connection is relatively new, there is a need for thoroughly investigating its properties and developing consistent design recommendations.

Background

The GSS connection consists of a prefabricated cap beam to which a stub pipe is welded, as shown in Fig. 1a. The stub pipe, larger in diameter than the column, acts as a socket into which the column can be inserted. The inner wall of the stub pipe contains many vertical lines of shear connectors, referred to as shear studs in this paper. The top of each pile section also has the same number of shear studs, as shown in Fig. 1a. In the field, shear studs are welded to the pile after driving and cutting it at the proper elevation. After inserting the pile into the stub (Fig. 1b), the moment-resisting connection is completed by pumping a high-strength, non-shrink

*Corresponding Author: Arjun Jayaprakash.
Email: arjunjayaprakashm@gmail.com
North Carolina State University, Raleigh, NC

Discussion period open till six months from the publication date. Please submit separate discussion for each individual paper. This paper is a part of the Vol. 2 of the International Journal of Bridge Engineering, Management and Research (© BER), ISSN 3065-0569.

flowable grout into the annular region (Fig. 1c). Fulmer, Kowalsky, and Nau[9] have previously shown that the GSS connection protects the weld and relocates the plastic hinge to the columns, as shown in Fig. 1d.

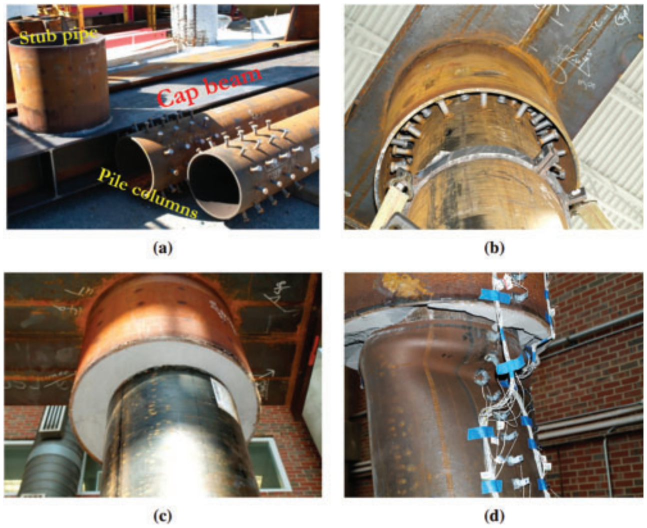

Figure 1. Stages of the GSS connection: (a) constituent components, (b) connection before grouting, (c) connection after grouting, (d) failure by plastic hinge relocation

The force-transfer mechanism within the GSS connection was previously[11] thought to be through full composite action of the GSS connection cross-section, in addition to the formation of complex compression struts between the shear studs on the column and the stub. The connection under tensile axial loading resulting from lateral loads in a two-column pier was considered as the critical design scenario. The column in such a connection is at risk of being pulled out of the socket if nothing resists the pullout. Given the capacity of a single shear stud, Fulmer et al.[11] calculated the total number of shear studs required to resist the axial tension demand in the connection by equally dividing the demand among all of the shear studs. The tension force demand in the connection was, in turn, calculated as the full axial yield force in the column section.

In the tests performed by Fulmer, Kowalsky, and Nau,[9] this design procedure led to a total of 96 shear studs of 19 mm (3/4 in.) diameter in a single GSS connection, 48 on the column and 48 on the stub pipe. All of the structural tests of two-column bridge piers with this connection led to successful outcomes. However, two important aspects regarding the GSS force-transfer mechanism have been realized since.

First, large-scale experiments performed as part of the present study show that the predominant mode of force transfer is not the composite action of the GSS connection. A revised force-transfer mechanism is discussed in this paper. This mechanism is similar to that observed by prior researchers[12–16] in the case of piles directly embedded into RC cap or footing elements. In these connections, the moment capacity is generally determined by the lower value between the plastic section moment of the pile and the moment due to the two normal forces developed as a result of columns bearing on the surrounding concrete.

Second, 96 shear studs per GSS connection are overly conservative. The full axial yield force of the column section is seldom mobilized. The bending of columns results in plastic hinging at the peak lateral load. Further cycles will result in reduced loads because of the pinching of the section. Therefore, the critical maximum axial load demand developed in the connection will be the tensile axial load corresponding to the peak lateral load in the system. This demand requires many fewer shear studs.

Objectives

There are two primary objectives of this paper. The first is to summarize the series of large-scale experiments that were performed to ascertain the structural behavior of the GSS connection. The focus therein is on identifying the structural limit states of the GSS connection to facilitate the optimum design and sound maintenance inspections in practice. The second objective is to formulate a design model for the GSS connection. This model must be able to estimate a lower bound of the moment capacity of the GSS connection.

Large Scale Experimental Setup

The experimental specimens (Fig. 2) were large-scale two-column steel bridge piers with GSS connections. The columns were 12.7 mm (1/2 in.) thick, 406 mm (16 in.) diameter round API 5L X52 PSL2 pipes, while the short stub pipes were 12.7 mm (1/2 in.) thick, 610 mm (24 in.) diameter round sections of the same material, which had a nominal yield strength of 360 MPa (52 ksi). The grout used to fill the annular void in the GSS connections was a high-strength cementitious grout with a manufacture-specified compressive strength (cylinder) of 55 MPa (8 ksi). The measured 28-day average cylinder strength of test samples was 73 MPa (10.6 ksi). Shear studs were welded on both the outside of the column top and the inside of the stub pipe in four rows. Along the circumference, each row had shear studs alternating between those on the column and those on the stub pipe. The total number of shear studs inside GSS connections varied for the different tests. This variation was partly to investigate the impact of the number of shear studs on the global system response, as discussed later.

The cap beam was a double-wide HP14x117 section, as described in the AISC[17] steel manual. The height of the center of the cap beam from the pin support was 3.40 m (11 ft 2 in.), and the center-to-center distance between the two columns was 3.66 m (12 ft). The steel bent was supported by two base shoes through pinned connections. The diameter of the steel pins was 127 mm (5 in.). Such a boundary condition mimics the point of contraflexure that develops in the moment profile of an actual bridge pier system. The base shoes themselves were prestressed to the laboratory strong floor using 35 mm (1–3/8 in.) diameter Dywidag bars, with a force of 667 kN (150 kips) per bar.

A 1957 kN (440 kips) capacity actuator mounted on the laboratory strong-wall was used to apply cyclic quasi-static

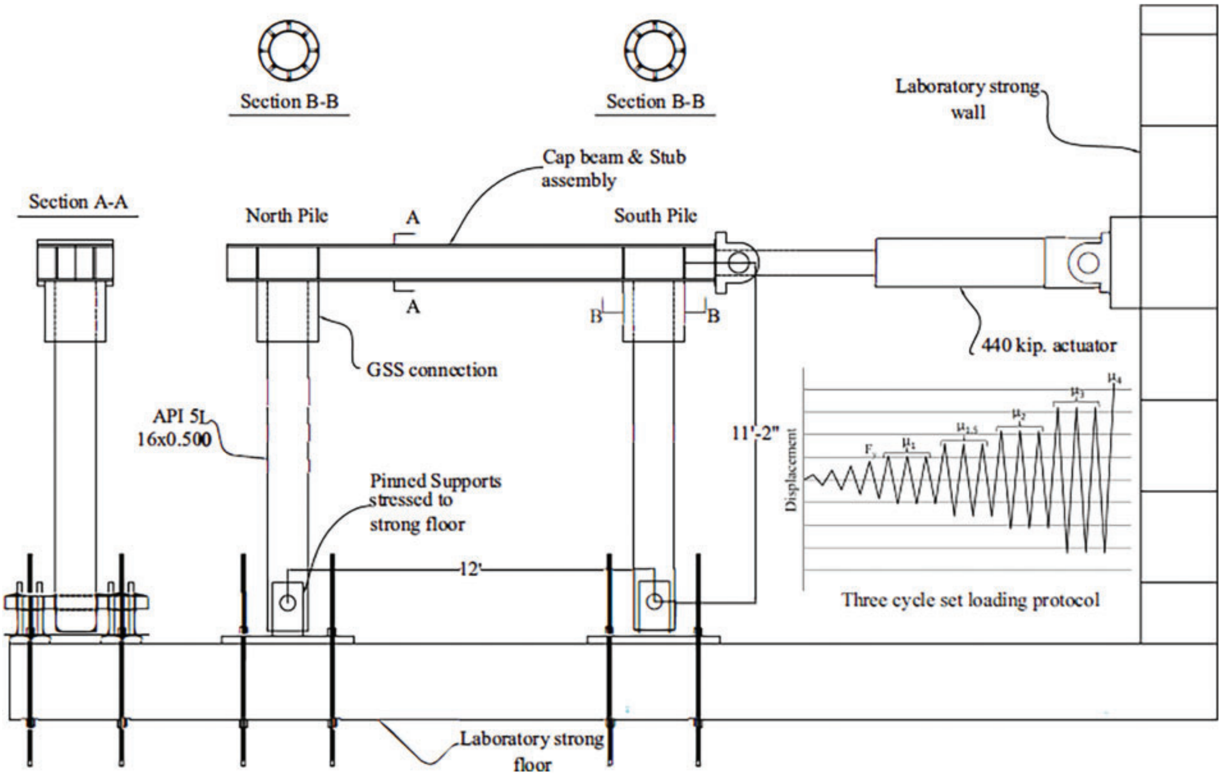

Figure 2. Laboratory large scale experiment setup

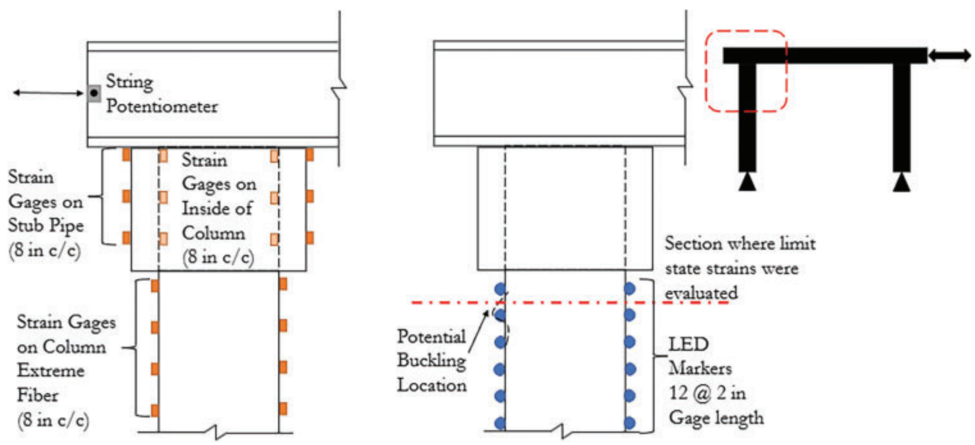

Figure 3. Instrumentation schematic for measurement of strains and system displacement at various limit states

lateral loading. A three-cycle set loading history, as shown in Fig. 2, was implemented by Jayaprakash.[18] This loading protocol[1,5,7,9,11, 19–21] consisted of three repeated load cycles at each displacement ductility level (F_y, μ_1, $\mu_{1.5}$, μ_2, and so on) until failure of the specimen.

The instrumentation scheme for the tests consisted of conventional electrical resistance strain gauges and string potentiometers (Fig. 3). Also utilized were Optotrak-Certus[22] sensors that detect LED markers attached to each specimen. This system allowed for the monitoring and recording of the three-dimensional coordinates of each marker in real-time. This coordinate data was post-processed to obtain displacement fields and, in turn, strains at locations of interest.

Details of each large-scale specimen in the series of experiments are provided in Table 1. Three parameters were varied among each test to answer key questions about the force-transfer mechanism in the GSS connection. These parameters were the grout mechanical properties, the number of shear studs (or the corresponding shear area), and the column embedment length into the connection. Details regarding the rationale and implementation of varying these parameters are described next.

Simulating grout deterioration

Notations SG and DG in the second column of Table 1 refer to standard grout (SG) and deteriorated grout, respectively. The grout used in SG specimens exhibited properties

Table 1. Test matrix used to determine the force-transfer mechanism of the GSS connection

No.	Name	Shear studs (nos.)	Stud area (mm^2)	Embed. length (mm)	Max. force (kN)	Reliable disp. ductility	Max. disp. ductility	Remarks
0	SG-96	96	1080	610	587	μ_3	μ_6	Adequate
1	SG-32	32	638	610	667	μ_3	μ_4	Adequate
2	DG-32	32	638	610	676	μ_3	μ_5	Adequate
3	DG-16	16	320	610	663	μ_3	μ_5	Adequate
4	DG-16-SE	16	320	406	472	None	N/A	Inadequate

resembling a newly constructed connection, whereas DG specimens contained grout with reduced strength and stiffness, representative of either long-term service or poor construction practices.[18] By subjecting the SG and DG specimens to the same test protocol, the impact of grout properties on the structural behavior of these two-column bridge bents could be determined.

Different methods were explored to emulate grout deterioration before settling on the use of aggregates called expanded polystyrene (EPS).[23] EPS is a stable, low-density foam consisting of discrete air voids in a polymer matrix. The elastic modulus of grout materials decreases with an increasing amount of EPS in their microstructure. Fig. 4 shows the results of the trial tests performed to determine this reduction in elastic modulus. A negative trend can be observed in the normalized elastic modulus with increasing volume replacement of EPS. A linear model was fitted to be used as a guideline to control the level of depletion in the large-scale tests.

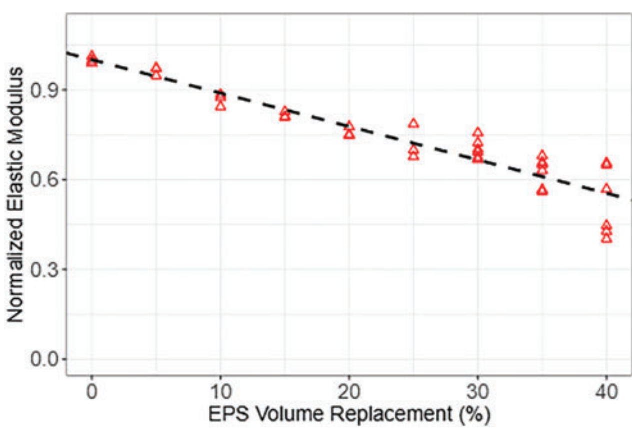

Figure 4. Elastic modulus normalized to value at 0% EPS plotted against EPS volume replacements for trial mixtures

Since E and f'_c are positively correlated, reducing the former to predefined values also resulted in the latter being reduced. There were two reasons why the modulus of elasticity (E), and not compressive strength (f'_c), was chosen as the primary variable to be reduced. The first is that, between the two, E is the parameter that is more difficult to reduce; that is, a 40% reduction in E will result in a significantly higher percentage reduction in f'_c. The second is that grout durability studies, such as those completed by Jayaprakash et al.,[10] utilize E as the parameter that defines the failure limit states.

Results from the tests of grout properties of the depleted grout in the two deteriorated test specimens are shown in Fig. 5. While there is some scatter, the GSS connections in these tests had, on average, a reduction in strength of 65% and in elastic modulus of 35% compared to those in the control specimens. The red dashed line in Fig. 5 shows the weighted mean of the measurements. The mean was calculated by weighting the measurements by the location of the sample along the height of the connection. Since the bottom of the connection was more important from a deterioration simulation standpoint, the measurements at the bottom were given a larger weight.

Variation of total shear stud area

The numeral that follows SG or DG in Table 1 represents the total number of shear studs per connection. Prior to this study, it was presumed that the force transfer within the GSS connection occurs through full composite action of the GSS connection cross-section and the associated formation of complex compression struts between the shear studs on the column and the socket.

Because both of these mechanisms are related to the number of shear studs present inside a connection, it follows that a significant reduction in the number of shear studs leads to inferior structural performance. This idea was tested by separately comparing the behavior of specimens SG-96 with SG-32 and DG-32 with DG-16, where the main difference between the compared specimens was the total stud shear area.

Note that test 0 was not performed as part of this study, but by Fulmer, Kowalsky, and Nau[9] on a similar specimen. However, it is included because of its relevance to the discussion regarding the impact of the total stud shear area on the structural performance of the GSS connection.

Variation of embedment length

The abbreviation SE in test 4 stands for the shorter embedment length used. As discussed earlier, many prior researchers have concluded that the amount of embedment length into the socket is a major factor that determines the integrity of socket connections. It was hypothesized that the same applies to the GSS connection. This hypothesis

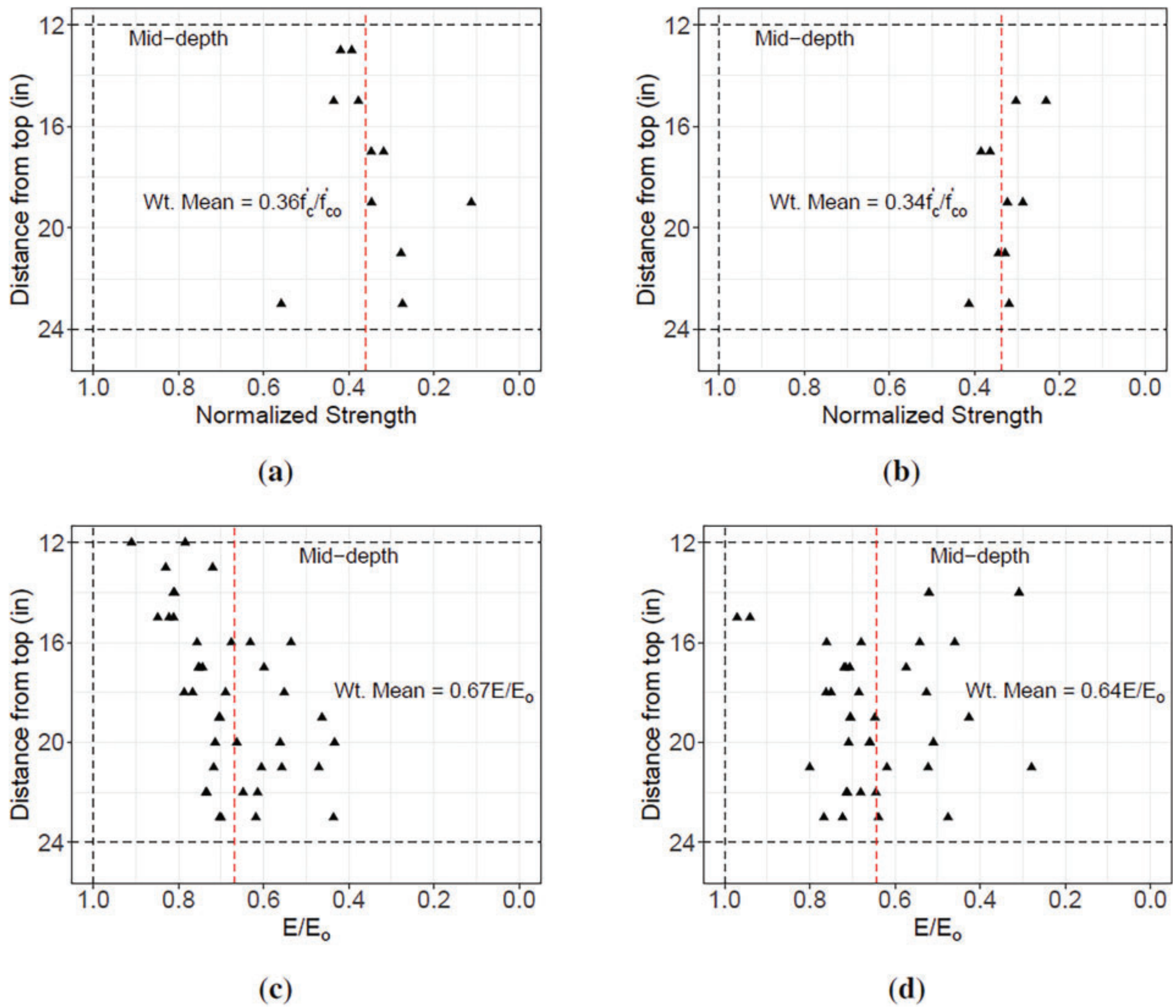

Figure 5. Results from the measurement of grout mechanical properties of the GSS connections in tests 2 and 3. (a, b) Compressive strength profile obtained from cubic samples from tests 2 and 3. (c, d) Dynamic elastic modulus profile obtained from disc samples from tests 2 and 3 (1 in. = 25.4 mm)

was tested by subjecting a specimen with short embedment length to the same test protocol and observing its behavior.

Experimental Results and Discussion

All of the experimental specimens where column plastic hinging was the failure mode exhibited common observable limit states. At or above ductility 1, the grout cracked radially at the neutral axis of the connection. The cracks were aligned transverse to the direction of loading, as shown in Fig. 6a. This cracking likely develops due to the following mechanism: many force components are mobilized inside the GSS connection under lateral loading, as shown in Fig. 7a. The column bears against the grout ring on the compression (C) side, creating a bearing pressure, as shown in Fig. 7b. This bearing pressure on the inside of the grout ring induces tensile hoop stress. When this tensile stress exceeds the tensile strength of the grout material, cracking ensues. Subsequently, the reaction of the grout ring on the column section results in ovalization of the section, which was visually observed in all specimens. While its extreme fibers are pushed inward, the circular section is pushed outward at the neutral axis. This causes compressive stresses to develop around the neutral axis region of the grout ring, which has already cracked. Previous cracking in this region allows further cracking and spalling.

As the tests progressed beyond ductility 1, a gap opened between the outside surface of the column and the inside surface of the grout ring. This observation is termed socket detachment (Fig. 6b). Due to section ovalization, the extreme ends are pushed inward, causing the tension side of the section to detach from the grout ring (Fig. 7c). Socket detachment became visible at ductility 1.5 in all three tests. The gap width became larger as the total force was increased. Consequently, the detachment at ductility 3 was wider than the corresponding size at ductility 1. It was observed that fewer studs and a weaker grout led to larger gap widths. Thus, a higher grout compressive strength and the presence of shear studs closer to the bottom of the connection can mitigate socket detachment. This is because section ovalization

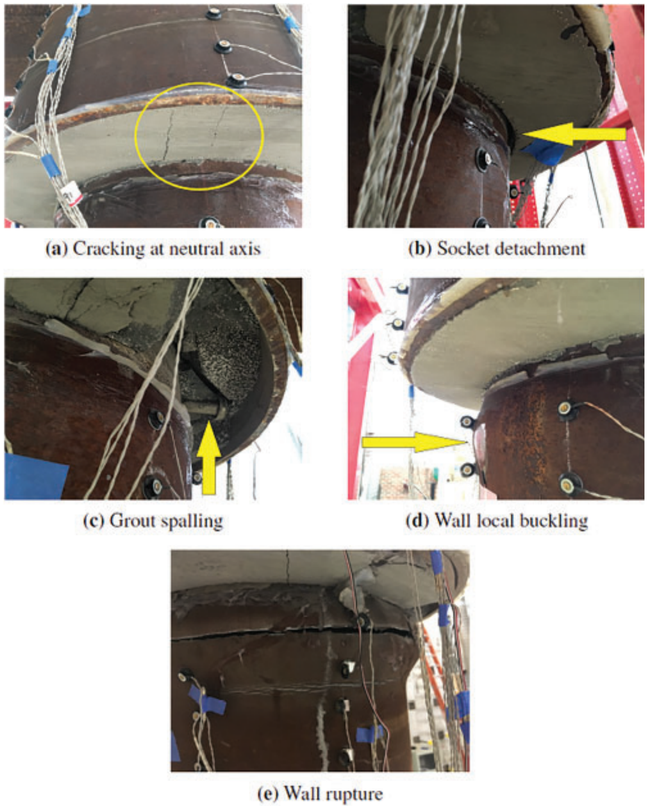

Figure 6. Visually identifiable limit states

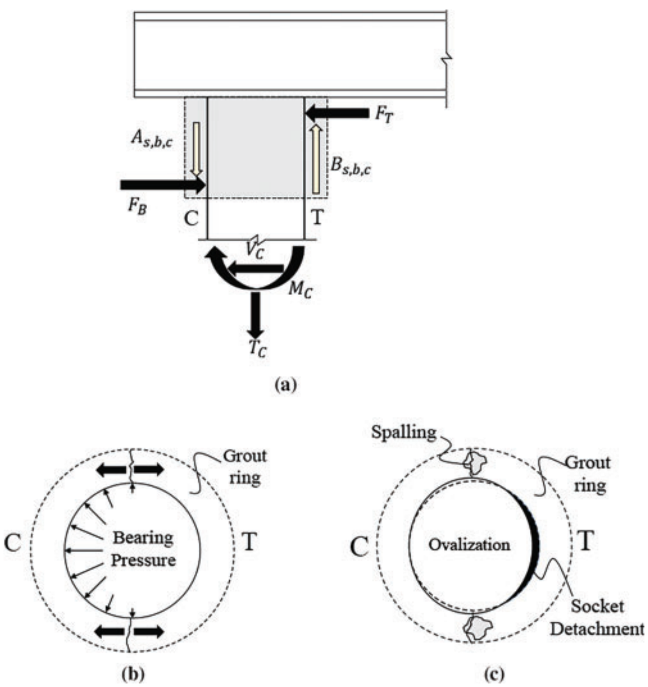

Figure 7. (a) Forces in the system and schematics to explain (b) cracking observed at the neutral axis, and (c) the socket detachment limit state of the GSS connection

is delayed by the surrounding grout and the bottom row of shear studs acting in compression and tension, respectively.

The grout on the extreme ends of the GSS connection, which are the regions farthest from the neutral axis under bending, spalled off after ductility 2 (Fig. 6c). As was discussed earlier, the presence of shear studs closer to the bottom of the connection delays the gap widening between the column and the grout ring. Because these shear studs are loaded axially in tension, the grout immediately surrounding them is also subjected to tensile stress. When this stress exceeds the tensile capacity of the surrounding grout, it cracks and spalls out of the connection.

Under cyclic loading, the column section reverses its compression and tension faces. Beyond a certain critical inelastic tensile strain, the pile wall has a propensity to buckle on the subsequent compression cycle. Pile wall buckling, followed by plastic hinge formation just beneath the GSS connection, is the desirable mode of failure for the bridge substructure systems discussed in this paper. Fig. 6d shows the first instance of visible pile wall buckling.

The ultimate limit state in the pile columns in a bridge substructure incorporating the GSS connection is pile wall rupture (Fig. 6e). This limit state occurs after a large number of inelastic cycles.

The structural tests provided a better understanding of the impact of each design parameter that was varied. This understanding served as the basis for the analytical force transfer model proposed in the following section.

Impact of grout mechanical properties

The two most important grout mechanical properties that contribute to the structural integrity of the GSS connection are the compressive strength (f'_c) and the elastic modulus (E). Nominally, a typical high-strength grout exhibits a 28-day compressive strength between 59 and 69 MPa (8.5–10 ksi) and an elastic modulus of 27.6–31.0 GPa (4000–4500 ksi). Test specimens with SGs in their GSS connections were tests 0 and 1. For tests 2 through 4, the GSS connections consisted of grout with reduced mechanical properties. This reduction was achieved by artificial means, as discussed earlier. Consequently, GSS connections in DG specimens exhibited a 65% reduction in f'_c and a 30% reduction in E (Fig. 5).

Subjecting specimens with SG and deteriorated grout to the same cyclic loading protocol did not result in significant differences in outcomes. Both test specimens underwent a ductile mode of failure in the form of plastic hinge formation below the GSS connection. Fig. 8 shows the comparison of the global force versus displacement cyclic response of these two tests. No clear distinction could be identified, either in the hysteresis curve (Fig. 8a) or the backbone envelope (Fig. 8b). The backbone envelope was obtained by picking only the points at peak displacement during the first cycle at each ductility level. A similar behavior was observed for specimen DG-16 where the structural response remained unaffected when compared to the specimen with SG.

The lack of sensitivity of the structural performance to the grout mechanical properties can be explained by the significant grout confinement present inside the GSS connection.

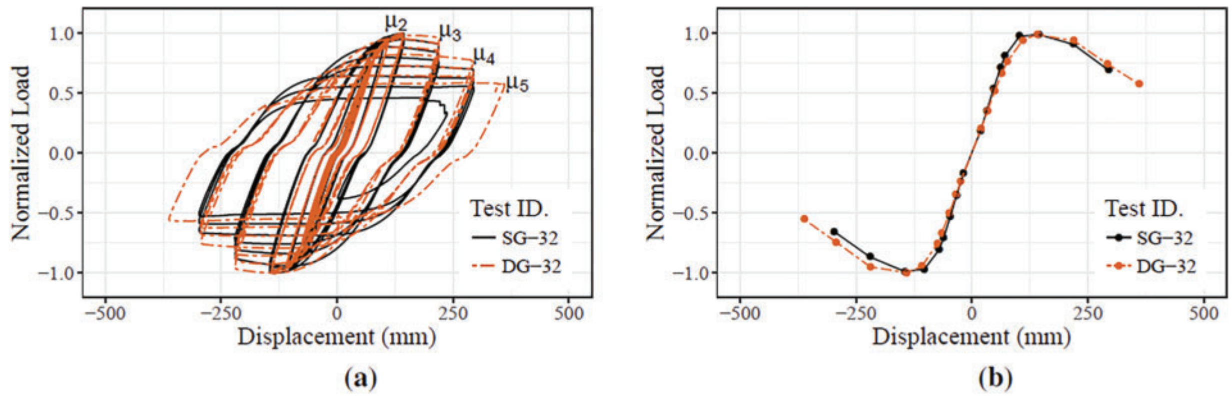

Figure 8. A comparison of the force–displacement response of specimens with standard (SG-32) and deteriorated (DG-32) grouts

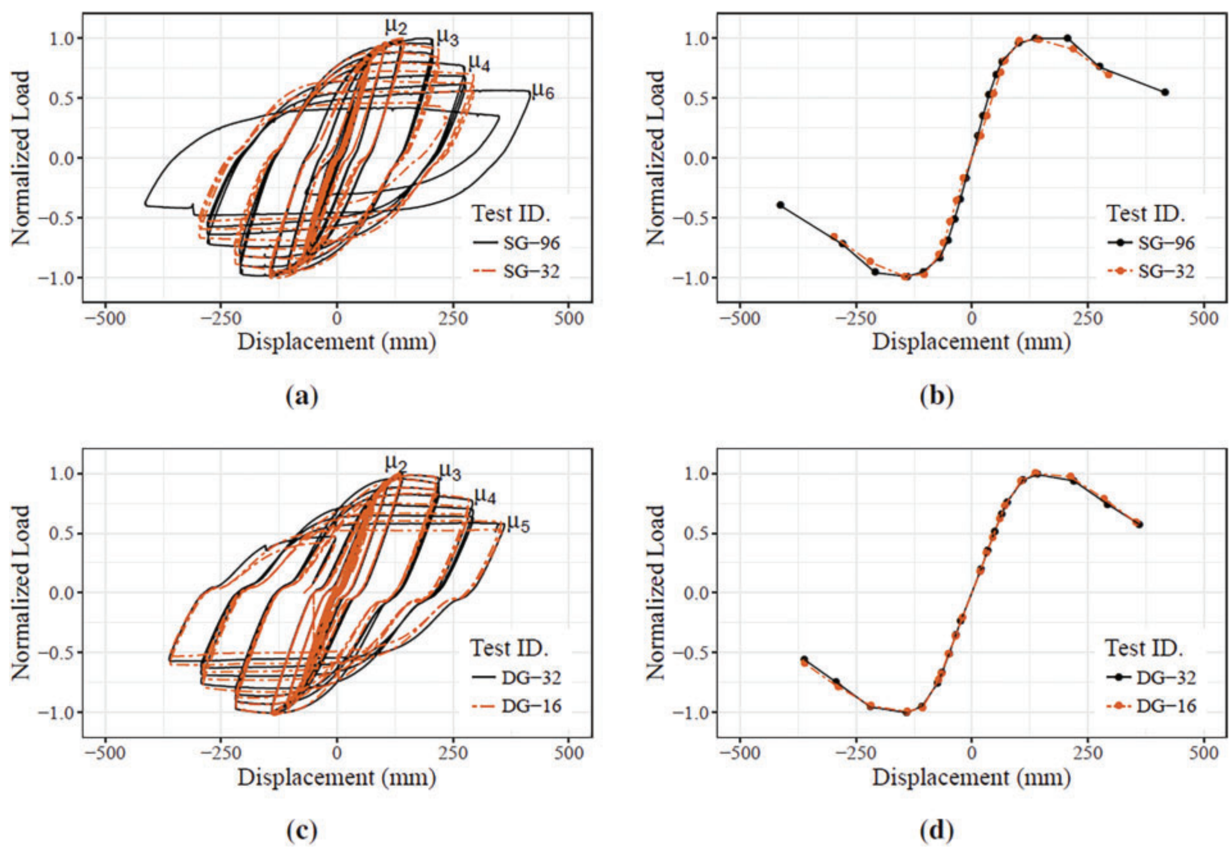

Figure 9. A comparison of the force–displacement response of specimens with different stud shear areas: 1080 mm^2 (42.4 in.^{2}) and 638 mm^2 (25.1 in.^{2}) (top), 638 mm^2 (25.1 in.^{2}) and 320 mm^2 (12.6 in.^{2}) (bottom)

As shown later by the proposed analytical model, the confined grout strength is adequate to successfully transfer the required forces, despite a much lower nominal strength of the grout.

Impact of stud shear area

Comparison of the structural response of specimens that varied only in terms of the number of shear studs indicated that the impact of the number of shear studs inside the GSS connection was also minimal (within the range of shear stud numbers used in this study), as can be inferred from Fig. 9. Despite the total stud shear area decreasing from 1080 mm^2 (42.4 in.^{2}) to 320 mm^2 (12.6 in.^{2}) in SG-96 and DG-16, respectively, the change in global structural behavior was barely noticeable.

Using information from prior literature[3,13,14,24,25] on piles embedded in adjoining RC members and the observation of a socket detachment limit state, as discussed earlier, it was surmised that the more likely force-transfer mechanism was socket action. Socket action is defined as the near rocking behavior of structural members inserted into sockets under loading. Because of this action, the column wall bears on

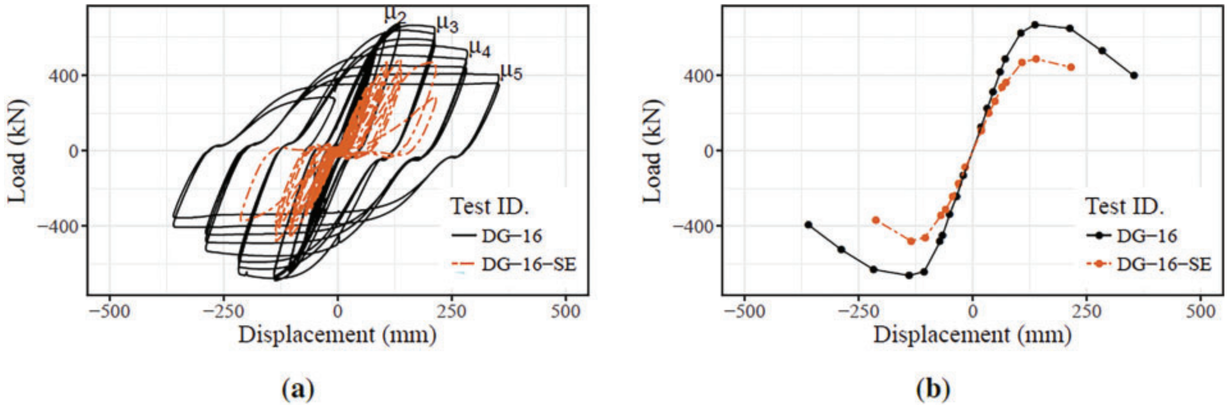

Figure 10. A comparison of the force–displacement response of specimens with variable embedment lengths

the inside of the grout ring at the top and bottom of the connection. The normal force pair, which is mobilized as a result, provides the path necessary for force transfer.

Impact of column embedment length (L_e)

For successfully resisting the moment demand on the GSS connection through socket action, the column embedment length (L_e) inside the connection becomes a key parameter. Test 4 (DG-16-SE) was therefore used to check this hypothesis by reducing the embedment length of the columns from 610 mm (24 in.) in test 3 (DG-16) to 406 mm (16 in.). When tested, there was a drastic shift in the structural behavior of the test 4 specimen, as shown in Fig. 10. The maximum strength of the pier decreased by 33%. There was neither plastic hinge formation nor ductile energy dissipation. Instead, the grout material reached its failure limit state first, resulting in progressive loss of grout during each successive cycle. This observation indicated that embedment length is a much more critical parameter in the design of the GSS connection compared to the number of shear studs and the grout mechanical properties. The analytical model proposed in this paper recognizes this dependence of the system on embedment length.

Analytical Model

A simple mechanics-based analytical model was sought to explain the force-transfer mechanism within the GSS connection. Based on empirical observations discussed earlier, the dominant mechanism is considered to be the moment resistance provided by the two bearing normal forces F_B and F_T, shown in Fig. 7a. Additionally, a small amount of resistance will also be provided by the two force components, $A_{s,b,c}$ and $B_{s,b,c}$, acting parallel to the column longitudinal axis. These two forces are a summation of contributions from different mechanisms, namely, the shear resistance of the studs (s), bond or friction between the outer steel circumference and the grout material (b), and compression struts which likely form between rows of shear studs (c).

The GSS connection is capacity protected, that is, it is designed to remain elastic or mostly undamaged beyond the point of plastic hinging in the columns. Hence, it can be conservatively assumed that the moment resistance is exclusively provided by the normal force pair F_B and F_T. This simplification is made to avoid calculating the marginal contribution from various other mechanisms individually. Furthermore, large-scale tests have shown that the contribution of shear studs to the overall structural performance of the bridge piers was significantly smaller compared to that of the socket action of the column.

The proposed analytical model for force transfer is discussed using a free body diagram of a column above the point of contraflexure, as shown in Fig. 11. In this figure, V_c is the shear force in the column at the point of contraflexure. The maximum value of this shear force can be calculated from the plastic moment (M_p) of the column section and the clear cantilever length (L_c), as shown in Eq. (1). A two-dimensional truss mechanism is assumed to transmit this shear force into the GSS connection. Under the load V_c, the column bears on the top and bottom of the inside grout surface of the GSS socket, mobilizing force reactions F_T and F_B, respectively.

$$V_c = \frac{M_p}{L_c} \tag{1}$$

The real distribution of stresses along the circumference of the connection is quite complex, especially with the presence of shear studs. An idealized representation of this distribution is shown in Fig. 11, as the oval-shaped black-colored arrows, where f'_{cm} is the maximum amplitude of this stress distribution. For the model, an equivalent uniform distribution of bearing stresses around the semi-circumference of the column is assumed, as shown by the light-red arrows in Fig. 11. If the total force calculated from both of these stress distributions are equated, the amplitude of the uniform distribution can be evaluated. This value can be considered as an equivalent average value of stress. If the value of this average stress is f'_{ca}, the total reaction force can be calculated from the typical ACI 318-19[26] stress block using Eq. (2), where L_e is the embedment length of the column inside the connection, D is the column diameter, and β_1 is a factor between 0.65 and 0.85, as provided in ACI 318-19.[26]

The allowable maximum stress (f'_{cm}) will depend on the degree of confinement and hence can be equated to the confined grout compressive strength (f'_{cc}). The confined grout

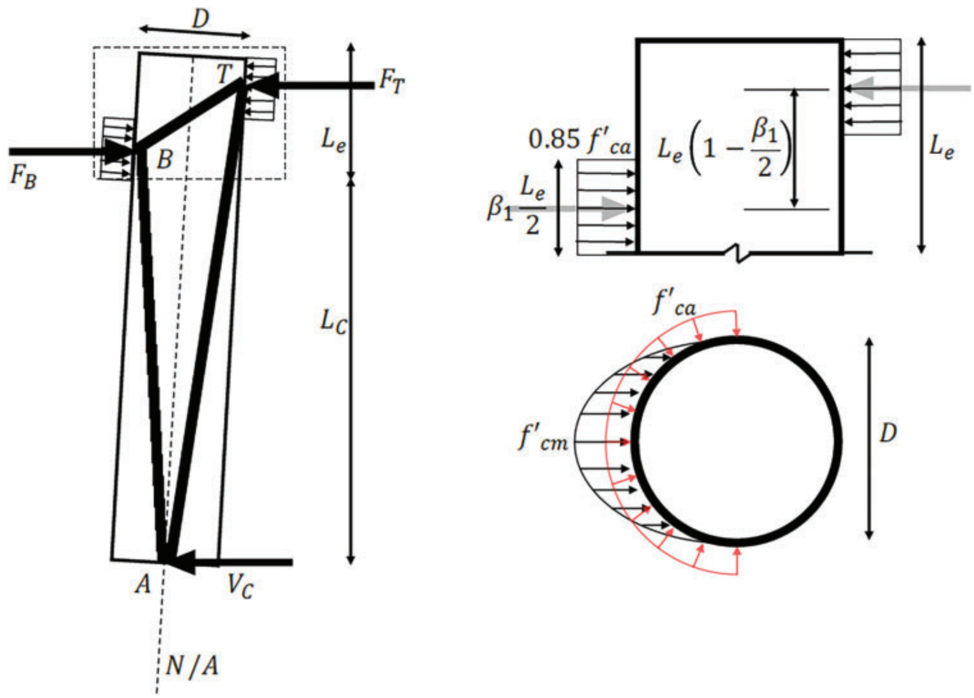

Figure 11. A schematic showing the truss mechanism of force transfer in a single column

compressive strength (f'_{cc}) can be estimated using Eq. (3), which was proposed by Richart, Brandtzaeg, and Brown.[27] In Eq. (3), f_l is the lateral confining pressure, which can be calculated using Eq. (4).

The average uniform stress (f'_{ca}) will be less than the true maximum stress experienced by the grout in the connection. With no prior information regarding the relationship between f'_{cm} and f'_{ca}, we recommend conservatively assuming that the maximum stress is double the average stress, as shown in Eq. (5). This relationship emerges if one assumes a linear variation of stresses around the circumference. It can be mathematically shown that the assumption of a linear variation of stresses produces the most conservative result compared to a higher-order variation

$$F = 0.85 f'_{ca}\beta_1 \frac{L_e}{2} D \tag{2}$$

$$f'_{cc} = f'_c + 4.1 f_l \tag{3}$$

$$f_l = \frac{2 f_{ymin} t_{stub}}{D_{stub}} \tag{4}$$

$$f'_{ca} \leq \frac{f'_{cc}}{2} \tag{5}$$

A relationship between the mobilized force F_B, in Fig. 11, and the column shear force (V_{Cmax}) can be established from the geometry of the column and the connection. In the free-body diagram of point A (Fig. 12a), it can be shown that F_{AB} is approximately equal to F_{AT} for typical column L/D ratios. The value of F_{AB} can, in turn, be calculated as

$$F_{AB} = \frac{V_c\left(L_c + L_e\left(1 - \frac{\beta_1}{4}\right)\right)}{D} \tag{6}$$

And in the free-body diagram of point B (Fig. 12b), F_{BT} can be evaluated as

$$F_{BT} = F_{AB}\frac{\sqrt{D^2 + L_e^2\left(1 - \frac{\beta_1}{2}\right)^2}}{L_e\left(1 - \frac{\beta_1}{2}\right)} \tag{7}$$

The bearing force F_B can then be calculated by adding the components of F_{AB} and F_{BT} in the same horizontal direction

$$F_B = F_{AB}\frac{D/2}{L_c + L_e\left(1 - \frac{\beta_1}{4}\right)} + F_{BT}\frac{D}{\sqrt{D^2 + L_e^2\left(1 - \frac{\beta_1}{2}\right)^2}} \tag{8}$$

Simplifying further by substituting the values of F_{AB} and F_{BT} as functions of V_C, the bearing force can be written as a function of the column shear force,

$$F_B = V_C\left(\frac{1}{2} + \frac{L_c + L_e\left(1 - \frac{\beta_1}{4}\right)}{L_e\left(1 - \frac{\beta_1}{2}\right)}\right) \tag{9}$$

When designing the connection, this bearing force must be kept below the bearing capacity calculated using Eq. (2). To design the GSS connection using capacity design principles, it is therefore sufficient to limit the maximum allowable column shear force, V_C, that satisfies the foregoing inequality. Consequently, Eq. (10) can be used to estimate the lower bound capacity of the GSS connection and thereby the

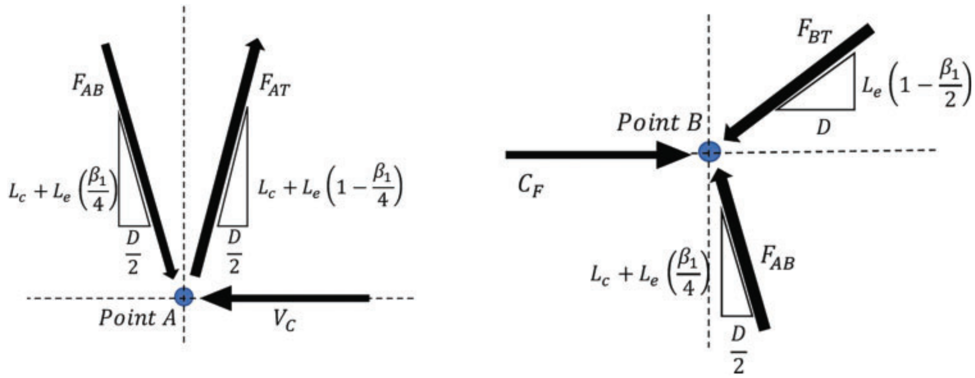

Figure 12. Free-body diagrams of points in the strut-and-tie model shown in Fig. 11: (a) point A and (b) point B

maximum allowable column shear force for successful plastic hinge formation in the column

$$V_C \leq \frac{0.85 f'_{ca}\beta_1 D\left(\frac{L_e}{2}\right)}{\left(\frac{1}{2} + \frac{L_c + L_e\left(1-\frac{\beta_1}{4}\right)}{L_e\left(1-\frac{\beta_1}{2}\right)}\right)} \tag{10}$$

For typical values, $\beta_1 = 0.8$ and $L_e = 0.2L_{tc}$, the above equation reduces to Eq. (11)

$$V_C \leq 0.008 f'_{ca} D L_{tc} \tag{11}$$

It must be noted that the axial force present in the column is considered separately in this model. The foregoing equations estimate the resistance of the GSS connection to the flexural demand only. The axial force is resisted by the grout-to-steel bond and the shear studs present inside the connection. The number of shear studs in the connection must be chosen to provide a positive load path to resist the seismically induced maximum axial tension force demand (Eq. (12)). This is to account for the unlikely event of losing all of the bond capacity over time or during a seismic event. In Eq. (12), n is the number of shear studs required both on the column and the socket, each. P_t is the axial tension demand on the GSS connection, f_u is the ultimate tensile strength of the shear stud, and A_{sc} is the cross-sectional area of a single shear stud

$$n = \frac{P_t}{0.6 f_u A_{sc}} \tag{12}$$

The type of axial force critical to the integrity of the GSS connection is the tension force that causes pullout. The magnitude of this tension force is often reduced because of the superstructure dead load. Therefore, it can be argued that the impact of axial force on the design of embedment length is much smaller than that of the bending moment input due to column flexure. However, it is recommended that a minimum number of shear studs always be provided for redundancy.

Application of the Analytical Model to Large-Scale Experiments

The proposed analytical model was developed using mechanics by making simplifying assumptions regarding force transfer in the GSS connection. Tests 3 and 4 produced empirical data to test the sufficiency of this model. Table 2 shows the step-by-step calculations performed to determine the capacity of the GSS connections in tests 3 and 4. The material properties f_y and f'_c were obtained by independent measurements of the steel coupons and grout samples, respectively, for each test. The remaining input variables are based on the geometry of the test setup. Fig. 13 shows the comparison of these dimensions for the two tests.

Table 2. Stepwise calculation of the capacity and demand in the GSS connections in tests 3 and 4

Step no.	Quantity (units)	Test 3	Test 4
1	f_{ymin} (MPa)	360	360
2	f_y (MPa)	469	476
3	t_{stub} (mm)	12.7	12.7
4	D_{stub} (mm)	610	610
5	D_{col} (mm)	406	406
6	f'_c (MPa)	25.5	28.3
7	$f'_{cc}(MPa)$	87	89.8
8	$f'_{ca}(MPa)$	43.5	44.9
9	β_1	0.8	0.8
10	L_e (mm)	610	406
11	L_c (mm)	2464	2667
12	$V_{capacity}$ (kN)	520	232
13	V_{demand} (kN)	356	322
14	D/C	0.68	1.40

The value of demand over capacity (D/C) for test 3, which had a longer embedment length of 610 mm (24 in.), was 0.68, while that of test 4, with a shorter embedment length of 406 mm (16 in.), was 1.40. It is therefore not surprising that the mode of failure for both tests was different. While test 3 failed in the desirable manner through plastic hinge

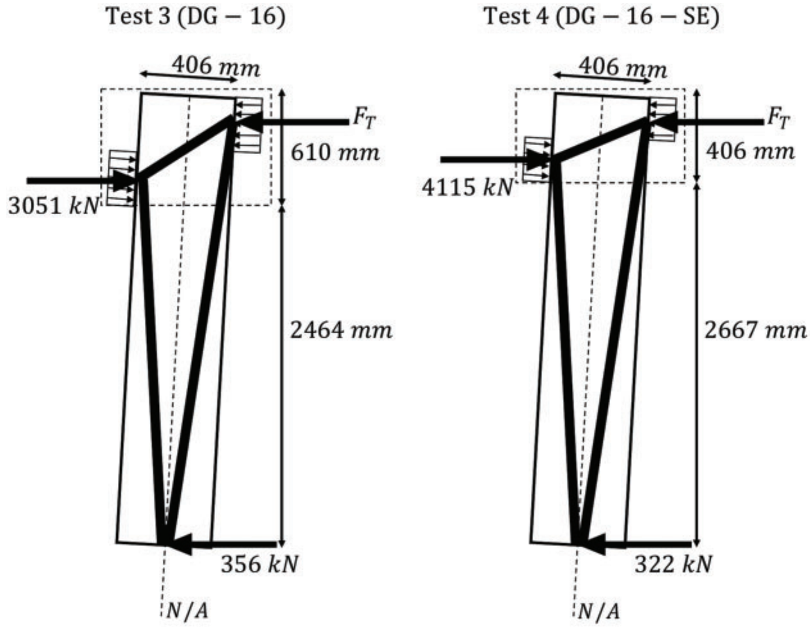

Figure 13. Comparison of the truss model for tests 3 and 4

formation, test 4 failed by grout spalling and the ensuing column rocking behavior, which was unable to mobilize plastic hinge formation.

The analytical model can also be used to determine a first approximation of the maximum lateral strength of the system. The shear force demand in a column is one of the input variables of the model. The D/C ratio for different values of shear force demand can therefore be calculated and plotted. Fig. 14a shows the result of such a calculation for both test 3 and test 4. The D/C ratio varies linearly with the applied shear force. The intersection of the two lines with the dashed line at the D/C ratio equal to 1.0 can be used to read the shear force capacity of the columns in tests 3 and 4, which are equal to 520 kN (117 kips) and 232 kN (52 kips), respectively. The total system lateral force capacity can then be calculated by multiplying the column capacities by the number of individual columns. Therefore the calculated system force capacity for tests 3 and 4 becomes 1041 kN (234 kips) and 463 kN (104 kips), respectively. The force–displacement backbone response of tests 3 and 4 is reproduced here in Fig. 14b. It can be seen that the maximum strength of the test 4 specimen is just above the value predicted by the model. On the other hand, full plasticity in the columns was mobilized in test 3 before reaching the predicted connection capacity. For a good design, the force–displacement backbone response should fall well below the estimated system lateral strength. The utility of this analytical model lies in its simplicity, as simple hand calculations can reveal potential deficiencies in design.

The proposed analytical model was used to perform a parametric study to ascertain sensitivity to the different variables of the model. This study was performed by varying the input variables in the model. Typical values were chosen for each variable in the study. Table 3 shows all of the input variables and their values used in the parametric study. First, the sensitivity of the demand over capacity ratio to each

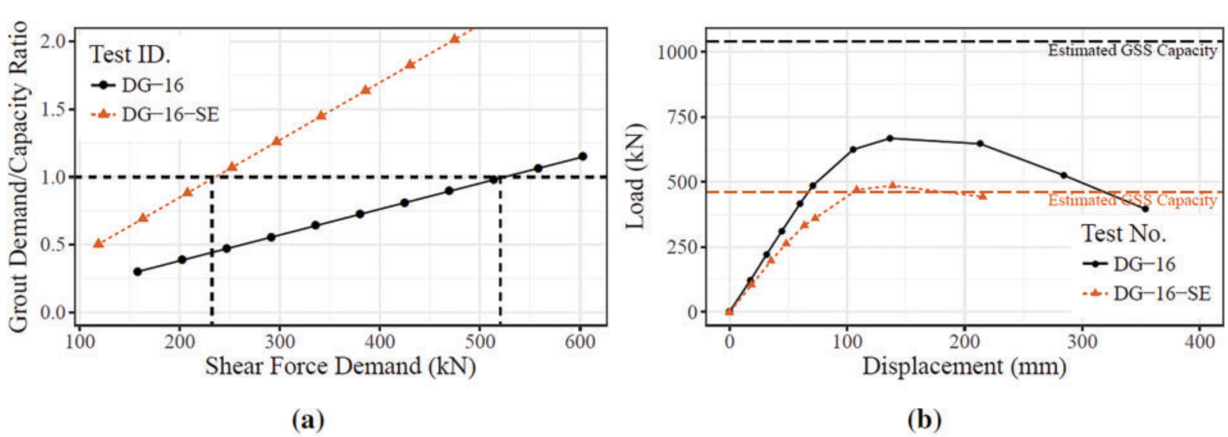

Figure 14. Illustrating the prediction of the GSS connection capacity: (a) Prediction; and (b) Comparison with empirical results

Table 3. Input variables and their values used in the parametric study

Input variable (units)	Values
Column pipe radius (mm)	152, 203, 254, 305, 356, 406
Column and stub pipe thickness (mm)	6.4, 12.7, 19.5, 25.4, 31.8
Column clear cantilever height (m)	1.52, 1.78, 2.03, 2.29, 2.54, 2.79, 3.05, 3.30, 3.56, 3.81
Embedment length (mm)	406, 457, 508, 559, 610, 660, 711, 762, 813, 864, 914, 965, 1020
Steel yield strength (MPa)	345, 414, 483
Grout compressive strength (MPa)	27.6, 34.5, 41.4, 48.3, 55.2, 62.1, 68.9, 75.8
β_1	0.65, 0.70, 0.75, 0.80, 0.85

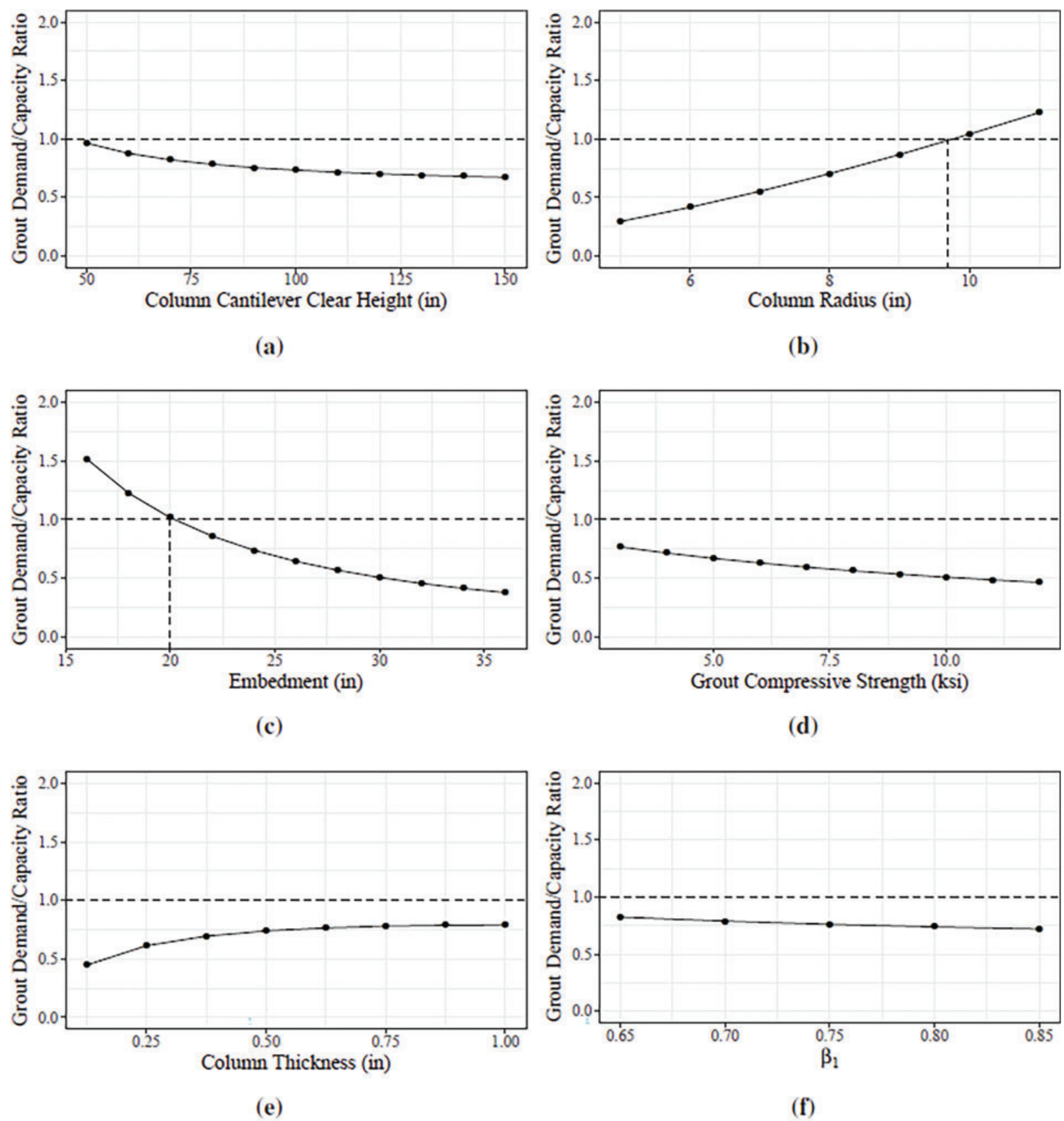

Figure 15. Sensitivity of the D/C ratio with respect to each variable in the parametric study, given that all of the other variables remain constant

of the variables was ascertained. Fig. 15 shows the typical variation in D/C ratio with respect to each variable. While keeping everything else constant, the embedment length and the column radius seemingly have a much larger impact on the D/C ratio. Therefore, while designing the GSS connection, it is recommended that these two variables be given the most consideration.

Eq. (10), derived previously, can be used to ensure that the GSS connection remains capacity protected under a seismic event. However, input variables to this equation, such as the column embedment length (L_e), column cantilever length (L_c), and column diameter (D), remain undetermined at the start of the design process. Results from the parametric study were therefore used to determine approximate geometric proportions of the bridge substructure to start with. Eq. (10) can then be used as a capacity check. If necessary, an iterative procedure must be applied to converge to an adequate design.

Two important geometric ratios, which, when correctly proportioned, lead to a satisfactory design, are the embedment length to total cantilever length (L_e/L_t) ratio and the embedment length to column diameter (L_e/D) ratio. Among more than 2 million different cases realized in the parametric study, a large sample consisting of 200,000 observations was randomly chosen to perform a simple statistical analysis to reveal trends in the variation of the aforementioned ratios

$$L_t = L_e + L_c \tag{13}$$

First, the D/C ratio was plotted against the L_e/L_t ratio. Note that the total cantilever length (L_t) is the sum of the embedment length (L_e) and the column clear cantilever length (L_c), as shown in Eq. (13). The length L_t, a function of the elevation of the superstructure, is generally known at the start of the design process. On average, when the L_e/L_t ratio increases, the D/C ratio decreases because longer embedment results in a longer lever arm for the resistive force couple developed in the GSS socket. Fig. 16a shows the D/C ratio plotted against the L_e/L_t ratio from the random sample obtained from the parametric study, which illustrates this conclusion. The shaded area in the figure corresponds to the region where the D/C ratio is between 0.6 and 0.9. It is recommended that the D/C ratio falls inside this range. Observations in the parametric study that fell within this range were plotted as a histogram, as shown in Fig. 16b. The L_e/L_t ratio between 0.2 and 0.3 had the most likelihood of achieving this desirable design condition. Note that the experimental specimens discussed in this study possessed a L_e/L_t ratio of 0.18.

Next, the D/C ratio was plotted against the L_e/D ratio. On average, when the L_e/D ratio increases, the D/C ratio decreases for the same reason as increasing embedment length. This is illustrated by Fig. 17a, which was obtained by plotting the D/C ratio against the L_e/D ratio of the random sample obtained from the parametric study. Again, the shaded area corresponds to the region where the D/C ratio is between 0.6 and 0.9. Observations in the parametric study that fell within the range were plotted as a histogram, as shown in Fig. 17b. The L_e/D ratio between 1.2 and 1.6 had the most likelihood of achieving this desirable design condition. Note that the experimental specimens discussed in this study possessed a L_e/D ratio of 1.5. Also note that the foregoing recommended range of L_e/D also contains the value of 1.3, which was recommended by Larosche et al.[13] for steel piles embedded in RC members.

Model limitations and future work

Although the analytical model provides a simple way to design the GSS connection, it involves many conservative assumptions. At this point, there is only a handful of experimental data for the GSS connection, which makes it unreasonable to propose a less conservative and more refined model. The proposed model must be applied to more experimental bridge substructure systems with GSS connections to ensure model sufficiency. Future studies should investigate the marginal contribution of the shear studs and grout bond/friction to the connection capacity. Applying seismic loading conditions through shake table tests can also provide valuable information in terms of more realistic demands in real scenarios. However, it must be noted that conservativeness in the design of a capacity-protected member, such as the GSS connection, is not necessarily a bad thing, nor does it increase the overall cost of construction. It is likely that

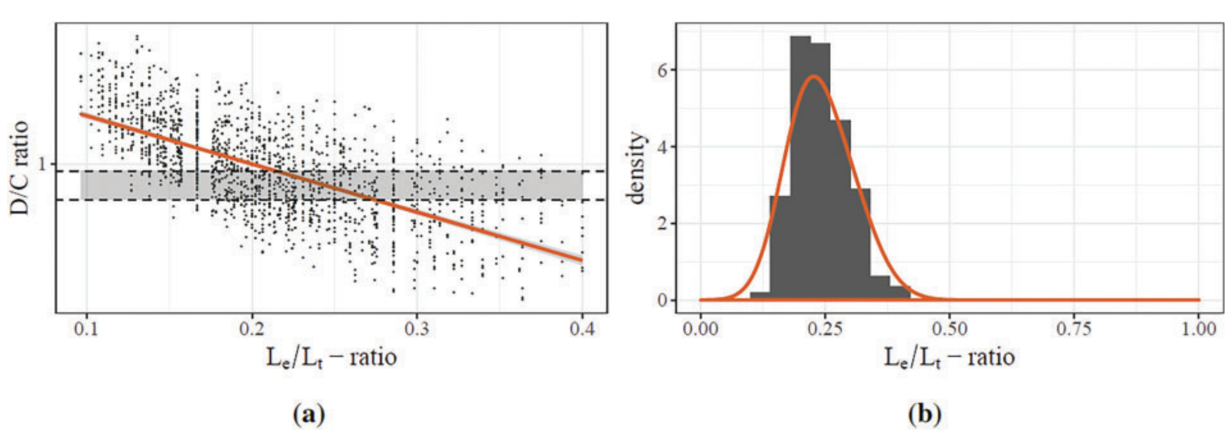

Figure 16. (a) D/C ratio versus L_e/L_t ratio from the parametric study. (b) Probability density of L_e/L_t ratios that led to optimum GSS connection design

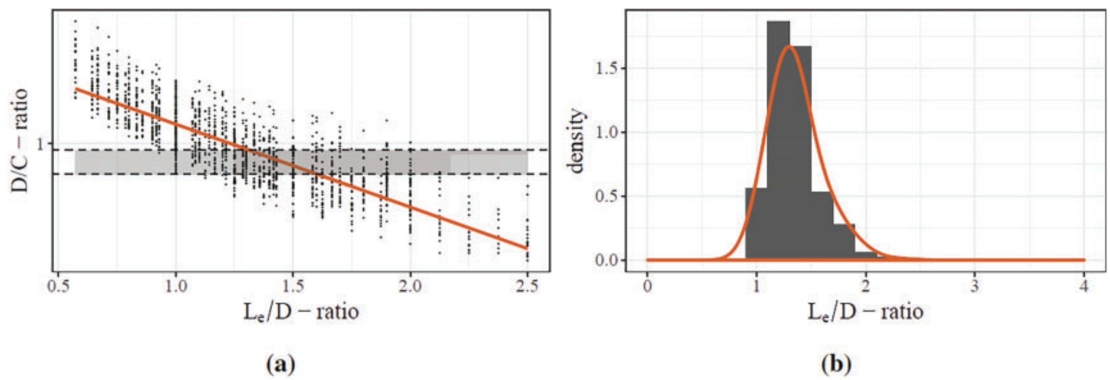

Figure 17. (a) D/C ratio versus L_e/D ratio from the parametric study. (b) Probability density of L_e/D ratios that led to optimum GSS connection design

the engineers employing the GSS connection in their design are satisfied by simply picking the recommended L_e/D and L_e/L_t ratios and checking for the important limit states.

For refining our understanding of the full force-transfer mechanism, there are a few different directions future research may take. It is still unclear what the optimum embedment length is for such systems. More large-scale specimens with variable L_e/D need to be tested. Another unanswered question is whether a higher number of shear studs or a higher grout strength partly alleviates problems associated with having a smaller embedment length.

The phenomenon of socket action requires further study. Additional tests can help quantify socket detachment and the variables it depends on, such as grout strength and stud configuration. Numerical simulation studies could be undertaken to reproduce the results of specimens that exhibited socket action.

And finally, more studies can be undertaken to determine the tensile capacity of the GSS connection. This would include determining the relative contribution of the shear resistance of the studs, bonding between the grout and the steel pipe, as well as the complex strut-and-tie mechanism that likely develops in the grout between the studs.

Summary and Conclusions

The work described in this paper began with the objective of better understanding the structural behavior of the GSS connection to develop a design method. The design procedure used by Fulmer, Kowalsky, and Nau[9] to determine the number of required shear studs in a GSS connection was overly conservative. Moreover, questions still lingered regarding the contribution of different design parameters to the overall structural response. Consequently, multiple large-scale specimens of two-column bridge bents were structurally tested.

Five different progressive limit states were identified for a well-designed GSS connection under system lateral loading. Because of hoop stress induced by bearing of the column on the inside of the grout ring, cracking initiates at the neutral axis. Subsequently, ovalization of the column section causes detachment of the grout ring from the column on the tension side. Further loading causes grout material on the extreme ends of the connection to spall. After progressing well into the inelastic range, the pile wall undergoes buckling below the connection. This local buckling is followed by plastic hinge formation and subsequent rupture of the pile wall. This progressive list of limit states may be used to qualitatively estimate the level of damage undergone by steel bridge substructures after a seismic event. Therefore, identification of these limit states was important for departments of transportation from a maintenance inspection standpoint.

Experimental observations were helpful in identifying the primary force-transfer mechanism in the GSS connection. It was found that the number of shear studs in the connection and the mechanical properties of the grout, both necessary components, are, however, insignificant relative to the importance of the embedment length of the column inside the GSS connection. In this regard, the decisive tests were DG-16 and DG-16-SE, wherein the former had an embedment length of 610 mm (24 in.) and the latter 406 mm (16 in.). It was found that when the connection fails to mobilize moment resistance through the normal force pair developed from column bearing on the grout ring, premature failure of the connection ensues, that is, the column remains straight and rocks within the grout annulus. This mechanism involving the moment resistance mobilized by the two normal forces is termed as socket action.

The socket action for a GSS connection column was approximated as a truss mechanism formulation that enabled the derivation of an equation to estimate the force capacity of the GSS connection. This model, when applied to the last two large-scale tests, yielded predictions that matched empirical observations. Next, a parametric study was performed using this model to (1) ascertain the sensitivity of this model to input variables and (2) determine approximate geometric proportions of bridge substructures that can lead to optimum design. It was determined that the embedment length to total cantilever length (L_e/L_t) ratio between 0.2 and 0.3, and the embedment length to column diameter (L_e/D) ratio between 1.2 and 1.6 can lead to an optimum GSS connection design.

Data Availability Statement

Some or all data, models, or code that support the findings of this study are available from the corresponding author upon reasonable request.

Acknowledegments

The research discussed in this paper was made possible by the financial support received from the Alaska Department of Transportation and Public Facilities (AKDOT) and the Department of Civil, Construction, and Environmental Engineering at North Carolina State University. None of the experimental work would have been completed on time without the technical staff, graduate students, and undergraduate students at the Constructed Facilities Laboratory.

References

[1] Cookson KA. *Seismic Performance of Steel Bridge Bent Welded Connections*. M.S. thesis, Raleigh, NC: NC State University; 2009.

[2] Kulkarni NG, Kasai A, Tsuboi H. Displacement based seismic verification method for thin-walled circular steel columns subjected to Bi-directional cyclic loading. *Eng Struct*. 2009;31(11):2779–2786.

[3] Harn R, Mays TW, Johnson GS. Proposed seismic detailing criteria for piers and wharves. In: *Ports 2010: Building on the Past, Respecting the Future*. 2010:460–469.

[4] Stephens J, McKittrick L. Final report: performance of steel pipe pile-to-concrete bent cap connections subject to seismic or high transverse loading. In: *FHWA/MT-05-001-8144*. Bozeman, MT: Montana Dept. of Transportation; 2005.

[5] Fulmer SJ, Kowalsky MJ, Nau JM. *Seismic Performance of Steel Pipe Pile to Cap Beam Moment Resisting Connections*. Rep. No. FHWA-AK-RD-13-02. North Carolina State University; 2013.

[6] Frandsen H. Seismic design of pile-supported wharves: effect of new steel strain limits in ASCE 61-19. *Ports 2019: Port Engineering*, Reston, VA: American Society of Civil Engineers; 2019:572–583.

[7] Fulmer SJ, Kowalsky MJ, Nau JM, Hassan T. *Ductility of Welded Steel Column to Steel Cap Beam Connections*. Rep. No. FHWA-AK-RD-10-04. North Carolina State University; 2010.

[8] Canha RMF, Ebeling EB, de Cresce El Debs ALH, El Debs MK. Analysing the base of precast column in socket foundations with smooth interfaces. *Mater Struct*. 2009;42(6):725–737. doi:10.1617/s11527-008-9416-4.

[9] Fulmer SJ, Kowalsky MJ, Nau JM. Grouted shear stud connection for steel bridge substructures. *J Construct Steel Res*. 2015;109(4):72–86. doi:10.1016/j.jcsr.2015.02.009.

[10] Jayaprakash A, Nau JM, Pour-Ghaz M, Kowalsky MJ. Durability of the grouted shear stud connection at low temperatures. *Rep. No. HFHWY00039*, North Carolina State University; 2019.

[11] Fulmer SJ, Nau JM, Kowalsky MJ, Marx EE. Development of a ductile steel bridge substructure system. *J Construct Steel Res*. 2016;118(4):194–206. doi:10.1016/j.jcsr.2015.11.012.

[12] Xiao Y, Wu H, Yaprak TT, Martin GR, Mander JB. Experimental studies on seismic behavior of steel pile-to-pile-cap connections. *J Bridge Eng*. 2006;11(2):151–159.

[13] Larosche A, Ziehl P, ElBatanouny MK, Caicedo J. Plain pile embedment for exterior bent cap connections in seismic regions. *J Bridge Eng*. 2013;19(4):04013016.

[14] Grilli D, Jones R, Kanvinde A. Seismic performance of embedded column base connections subjected to axial and lateral loads. *J Struct Eng*. 2017;143(5):04017010.

[15] Hammett S. *Theoretical Moment-Rotation Curve for Steel Piles Embedded in Concrete*. M.S. thesis. Auburn, AL: Auburn University; 2017.

[16] Shama AA, Mander JB, Blabac BA, Chen SS. Seismic investigation of steel pile bents: I. Evaluation of performance. *Earthquake Spectra*. 2002;18(1):121–142.

[17] AISC. *Steel Construction Manual*. Chicago, Illinois: American Institute of Steel Construction; 2005.

[18] Jayaprakash A. Recommendations for durability and seismic design of an external socket connection in steel bridge substructures. PhD thesis. North Carolina State University, Raleigh, USA; 2020. https://www.lib.ncsu.edu/resolver/1840.20/37366.

[19] Goodnight JC, Kowalsky MJ, Nau JM. Strain limit states for circular RC bridge columns. *Earthquake Spectra*. 2016;32(3):1627–1652. doi:10.1193/030315EQS036M.

[20] Krish ZF, Kowalsky MJ, Nau JM. Seismic repair of circular reinforced concrete bridge columns by plastic hinge relocation with grouted annular ring. *J Earthquake Eng*. 2019;25(12):2371–2405. doi:10.1080/13632469.2019.1688205.

[21] Barcley L, Kowalsky M. Seismic performance of circular concrete columns reinforced with high-strength steel. *J Struct Eng*. 2020;146(2):04019198. doi:10.1061/(ASCE)ST.1943-541X.0002452.

[22] Optotrak-Certus. *Optotrak Certus Spatial Measurement System*. NDI Measurement Sciences; 2007.

[23] Ravindrarajah RS, Tuck AJ. Properties of hardened concrete containing treated expanded polystyrene beads. *Cem Concr Composit*. 1994;16(4):273–277.

[24] Lehman DE, Roeder CW. Foundation connections for circular concrete-filled tubes. *J Construct Steel Res*. 2012;78:212–225.

[25] Stephens MT, Lehman DE, Roeder CW. Design of CFST column-to-foundation/cap beam connections for moderate and high seismic regions. *Eng Struct*. 2016;122:323–337.

[26] ACI:318-19. *Building Code Requirements for Structural Concrete (ACI 318-19) and Commentary*. Farmington Hills, Michigan: American Concrete Institute; 2019.

[27] Richart FE, Brandtzaeg A, Brown RL. *A Study of the Failure of Concrete Under Combined Compressive Stresses*. Urbana-Champaign, Illinois: University of Illinois at Urbana Champaign, College of Engineering; 1928.

Supplementary Materials

Design Example

Problem statement

The roadway bridge shown in Fig. 18 is in a seismically active region. The GSS connections in the two-column bridge substructures are to be designed. The columns were designed according to the seismic provisions of the region. During column design, the embedment length to total length (L_e/L_t) ratio was assumed to be 0.2. The resulting columns are hollow circular sections 460 mm (18 in) in diameter and 12.7

mm (0.5 in) in wall thickness. The column length above the point of contraflexure up to the cap-beam soffit is 4.56 m (15 ft). The point of contraflexure is idealized in Fig. 18 as pinned supports. The centerline span of the cap-beam was derived from the geometry of the deck and is equal to 5 m.

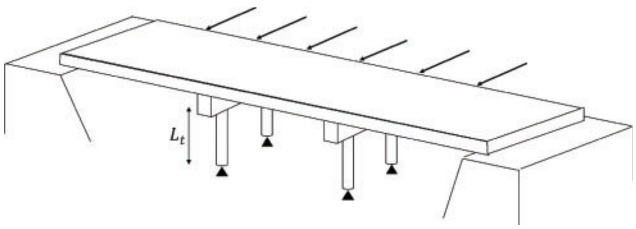

Figure 18. A typical bridge.

Solution

Step 1

The embedment length (L_e) and the clear cantilever length (L_c) of the column can be determined from the given values of L_t = 4.56 m and L_e/L_t = 0.2, using Eq. (13).

$$L_e = 912 \text{ mm}$$
$$\approx 900 \text{ mm}$$
$$L_c \approx 3660 \text{ mm}$$

Step 2

The shear force demand (V_p) in one column can be obtained using Eq. (1). Assuming column yield strength (f_y) as 359 MPa, and material overstrength factor (ω) of 1.3, V_p can be calculated as follows.

$$f_{y-exp} = \omega f_y$$
$$= 467 \text{ MPa}$$
$$M_p = f_{y-exp} Z$$
$$= 1170 \text{ kNm}$$
$$V_p = \frac{M_p}{L_c}$$
$$= 320 \text{ kN}$$

where Z is 2.51×10^6 mm^3, the plastic section modulus of the hollow circular steel cross-section.

Step 3

The diameter of the stub pipe forming the socket can be determined using the recommended range for L_e/D ratio. The diameter of the stub pipe may also be controlled by the minimum length of the shear studs chosen for design. Until then, a convenient L_e/D ratio between 1.2 and 1.6 may be chosen. This example proceeds by choosing 1.4.

$$D_{stub} = 1.4 \times 460$$
$$= 644 \text{ mm}$$
$$\approx 650 \text{ mm}$$

Step 4

Shear force capacity of the GSS connection can then be estimated using Eq. (11) and checked against the calculated demand. Assuming a 28-day grout compressive strength (f_c') of 65 MPa, which is typical for high-strength grouts, the GSS connection capacity can be calculated as follows.

$$f_l = \frac{2 f_{ymin} t_{stub}}{D_{stub}}$$
$$= 14.5 \text{ MPa}$$
$$f_{ca}' = \frac{1}{2}\left[f_c' + 4.1 f_l\right]$$
$$= 62.0 \text{ MPa}$$
$$V_C = 0.008 f_{ca}' D L_t$$
$$= 1040 \text{ kN}$$

Since, V_C is much greater than V_p, the current geometric proportions are adequate.

Step 5

To determine the size and number of shear studs, the maximum seismically induced tensile axial load must be calculated. This axial tension may either be determined from the structural model of the bridge or be conservatively determined by a simple calculation, as shown below. The conservatism arises from the neglect of the gravity load on the column. Note that the critical condition for shear stud design is the pull out of the column because of axial tension.

The maximum lateral force on a single bridge bent can be calculated as two times the maximum shear force evaluated for a single column. Assuming pinned supports at the point of contraflexure, the overturning moment can therefore be calculated as

$$M_{OT} = 2 V_p L_t$$
$$= 2920 \text{ kNm}$$

This overturning moment must be resisted by the equal but opposite axial forces in the columns. Thus, the seismically induced axial tension can be calculated as

$$P_t = \frac{M_{OT}}{L_{cbc}}$$
$$= 583 \text{ kN}$$

where L_{cbc} is the span of the cap-beam centerline, which is 5 m.

Step 6

It is recommended that the distribution of shear studs be determined first. Assuming four vertical lines of shear studs on four diametrically opposite sides of the column and each row spaced at 125 mm from each other, one can determine the total number of shear studs resisting the tension force. Subsequently, the required total shear area may be calculated by dividing the total axial force equally to all of the shear studs.

$$n = 4 \text{ lines} \times 7 \text{ rows}$$

$$= 28 \text{ nos.}$$

$$A_{sc} = \frac{P_t}{0.6nf_u}$$

$$= 42.2 \text{ mm}^2$$

where f_u is the ultimate tensile strength of one shear stud and is usually provided by the manufacturer. Here, f_u is assumed as 827 MPa. A shear area of 42.2 mm^2 corresponds to a shear stud diameter of 8 mm, which is smaller than minimum stud diameter that was tested. Hence, to satisfy minimum requirements, 19 mm shear studs may be used.

Final Design

GSS Embedment Length = 900 mm

Socket Diameter = 650 mm

Shear Studs = 56 nos (28 each on column and stub pipe)

Stud Diameter = 19 mm

Min. 28-day Grout Compressive Strength = 65 MPa